arXiv:2003.14075v2 [cond-mat.stat-mech] 17 Jun 2020

Three-dimensional monopole-free CP^{N-1} models

Andrea Pelissetto
Dipartimento di Fisica dell'Università di Roma Sapienza and INFN Sezione di Roma I, I-00185 Roma, Italy

Ettore Vicari
Dipartimento di Fisica dell'Università di Pisa and INFN Largo Pontecorvo 3, I-56127 Pisa, Italy

(Dated: January 4, 2022)

We investigate the phase diagram and the nature of the phase transitions of three-dimensional monopole-free CP^{N-1} models, characterized by a global U(N) symmetry, a U(1) gauge symmetry, and the absence of monopoles. We present numerical analyses based on Monte Carlo simulations for $N = 2$, 4, 10, 15, and 25. We observe a finite-temperature transition in all cases, related to the condensation of a local gauge-invariant order parameter. For $N = 2$ we are unable to draw any definite conclusion on the nature of the transition. The results may be interpreted in terms of either a weak first-order transition or of a continuous transition with anomalously large scaling corrections. However, the results allow us to exclude that the transition belongs to the O(3) vector universality class, as it occurs in the standard three-dimensional CP^1 model without monopole suppression. For $N = 4, 10, 15$, the transition is of first order, and significantly weaker than that observed in the presence of monopoles. For $N = 25$ the results are consistent with a conventional continuous transition. We compare our results with the existing literature and with the predictions of different field-theory approaches. They are consistent with the scenario in which the model undergoes continuous transitions for large values of N, including $N = \infty$, in agreement with analytic large-N calculations for the N-component Abelian-Higgs model.

I. INTRODUCTION

Models of scalar fields with U(1) gauge symmetry and U(N) global symmetry have been extensively studied with the purpose of identifying the nature of their different phases and transitions. They emerge as effective theories of superconductors and superfluids and of quantum SU(N) antinferromagnets [1–8]. In particular, three-dimensional (3D) classical models with $N = 2$ are supposed to describe the transition between the Néel and the valence-bond-solid state in two-dimensional antiferromagnetic SU(2) quantum systems [9–15], that represent the paradigmatic models for the so-called deconfined quantum criticality [16].

In the last twenty years there has been an extensive discussion on the nature of the transition occurring in this class of quantum models and in their classical counterparts. It has been realized that the nature of the transition depends crucially on topological aspects, for instance the Berry phase in the quantum case, the compact/noncompact nature of the gauge fields and the presence/absence of monopoles in the classical setting. In this paper we wish to understand the role that topological defects play in the simplest classical model with U(1) gauge symmetry, the lattice CP^{N-1} model. The fundamental fields are complex N-component unit vectors $\boldsymbol{z}_{\boldsymbol{x}}$, associated with the sites of a regular lattice — we will consider cubic lattices — and U(1) gauge variables $\lambda_{\boldsymbol{x},\mu} = e^{i\theta_{\boldsymbol{x},\mu}}$ associated with the lattice links. The corresponding Hamiltonian is [17–19]

$$H = -N \sum_{\boldsymbol{x},\mu} \left(\bar{\boldsymbol{z}}_{\boldsymbol{x}} \cdot \lambda_{\boldsymbol{x},\mu}\, \boldsymbol{z}_{\boldsymbol{x}+\hat{\mu}} + \text{c.c.} \right), \tag{1}$$

where the sum is over all lattice sites $\boldsymbol{x}$ and directions μ ($\hat{\mu}$ are the corresponding unit vectors). The partition function is

$$Z = \sum_{\{\boldsymbol{z}_{\boldsymbol{x}}, \lambda_{\boldsymbol{x},\mu}\}} e^{-\beta H}. \tag{2}$$

The factor N in the Hamiltonian (1) is introduced for convenience; with this definition, the large-N limit is defined by taking $N \to \infty$ keeping β fixed. One can easily check that Hamiltonian (1) is invariant under the global U(N) transformations

$$\boldsymbol{z}_{\boldsymbol{x}} \to U \boldsymbol{z}_{\boldsymbol{x}}, \qquad U \in \mathrm{U}(N), \tag{3}$$

and the local U(1) gauge symmetry

$$\boldsymbol{z}_{\boldsymbol{x}} \to e^{i\alpha_{\boldsymbol{x}}} \boldsymbol{z}_{\boldsymbol{x}}, \qquad \lambda_{\boldsymbol{x},\mu} \to e^{i\alpha_{\boldsymbol{x}}} \lambda_{\boldsymbol{x},\mu} e^{-i\alpha_{\boldsymbol{x}+\hat{\mu}}}. \tag{4}$$

The model has a continuous transition for $N = 2$ in the O(3) universality class, while the transition is of first order for any $N \geq 3$ [20, 21]. Note that the transition is not continuous even for $N = \infty$, in disagreement with analytic calculation [18, 20] performed for this model (see Ref. [21] for a discussion).

As we already mentioned, we expect the critical behavior to depend on topological properties. Topological defects like monopoles (or hedgehogs) are supposed to be relevant in determining the phase behavior. For instance, the disordered phase and the corresponding phase transition is absent in an O(3) vector model in which all hedgehogs are suppressed [22, 23], while a partial suppression leads to a phase transition that appears different from the Heisenberg one [23, 24]. Analogously, the failure of the usual analytic calculations in the large-N limit for model (1) has been ascribed to the presence of topologically nontrivial configurations that forbid the ordering of the gauge fields in the high-temperature phase [21, 25].

To explore the role that topological defects play in classical scalar U(1) gauge systems, we consider the monopole-free CP^{N-1} ($MFCP^{N-1}$) model. In this model the statistical average is performed by summing only over the gauge-field configurations in which monopoles are absent, where monopoles are defined using the De Grand-Toussaint prescription [26]. The model we consider here is strictly related with the Abelian Higgs model with noncompact gauge fields, which is often referred to as noncompact CP^{N-1} model in the literature on deconfined quantum criticality, see, e.g., Refs. [7, 24], and, for $N = 2$, to the O(3) model with hedgehog suppression discussed in Refs. [22–24]. They all share the same global symmetry group and are characterized by the suppression of topological defects.

We consider different values of N, i.e. $N = 2, 4, 10, 15$ and 25. In all cases, we observe a finite-temperature transition associated with the local order parameter

$$Q^{ab}_{\boldsymbol{x}} = \bar{z}^a_{\boldsymbol{x}} z^b_{\boldsymbol{x}} - \frac{1}{N}\delta^{ab}, \tag{5}$$

which is a gauge-invariant hermitian and traceless $N \times N$ matrix that transforms as

$$Q_{\boldsymbol{x}} \to U^\dagger Q_{\boldsymbol{x}}\, U \tag{6}$$

under the global U(N) transformations (3).

We analyze the nature of the transition using finite-size scaling (FSS) methods. In all cases, we observe that the suppression of monopoles changes significantly the behavior of the system. For $N = 2$ our results are definitely not consistent with an O(3) continuous transition. Monopoles are essential to guarantee the Heisenberg nature of the transition for $N = 2$. We are however unable to establish the order of the transition for the $MFCP^1$ model. Our data are consistent with a very weak first-order transition or with a continuous transition with large scaling corrections. For $N = 4, 10, 15$ the transition is of first order, as in the model with monopoles, but is significantly weaker. Finally, for $N = 25$, we observe a continuous transition. The latter result implies the existence of a value N_c such that the first-order transition observed for $4 \le N \le 15$ turns into a continuous one as N increases beyond N_c. This leads us to conjecture that the $MFCP^{N-1}$ model has a continuous transition in the large-N limit, as predicted by a perturbative analysis of the Abelian-Higgs field theory [18, 27].

The paper is organized as follows. In Sec. II we define the 3D $MFCP^{N-1}$ model we consider, while in Sec. III we define the basic observables that are determined in the Monte Carlo simulations. The numerical results are presented in Sec. IV. In Sec. IV A we present the results for $N = 4, 10, 15$, which are all consistent with a first-order transition. In Sec. IV B we discuss the results for $N = 2$. In spite of the large simulated systems, we are unable to draw any conclusion on the order of the transition. Finally, in Sec. IV C we discuss the results for $N = 25$, which are definitely consistent with a continuous transition. Finally, in Sec. V we summarize our main results and compare them with the existing relevant literature.

II. THE LATTICE $MFCP^{N-1}$ MODEL

In our study we consider the CP^{N-1} model with Hamiltonian (1) on a cubic lattice with periodic boundary conditions. We define monopoles and antimonopoles using the De Grand-Toussaint prescription [26]. In this approach one starts from the noncompact lattice curl $\Theta_{\boldsymbol{x},\mu\nu}$ associated with each plaquette

$$\Theta_{\boldsymbol{x},\mu\nu} = \theta_{\boldsymbol{x},\mu} + \theta_{\boldsymbol{x}+\hat{\mu},\nu} - \theta_{\boldsymbol{x},\nu} - \theta_{\boldsymbol{x}+\hat{\nu},\mu}, \tag{7}$$

where $\theta_{\boldsymbol{x},\mu}$ is the phase associated with $\lambda_{\boldsymbol{x},\mu}$, $\lambda_{\boldsymbol{x},\mu} = e^{i\theta_{\boldsymbol{x},\mu}}$. Here μ and ν are the directions that identify the plane in which the plaquette lies. Note that $\Theta_{\boldsymbol{x},\mu\nu}$ is antisymmetric in μ and ν, so that we associate two different quantities that differ by a sign with each plaquette. Let us now consider a closed lattice surface S made of elementary plaquettes. We associate $\Theta_{\boldsymbol{x},\mu\nu}$ with each plaquette $P = (\boldsymbol{x}, \mu\nu)$, ordering μ and ν so that the unit vector $\hat{\mu} \times \hat{\nu}$ points outward with respect to the surface. It is then easy to verify that

$$\sum_{P\in S} \Theta_{\boldsymbol{x},\mu\nu} = 0. \tag{8}$$

Indeed, with the chosen orientation of the plaquettes, each variable $\theta_{\boldsymbol{x},\mu}$ [$(\boldsymbol{x}, \mu)$ is a link belonging to S] appears twice in the sum (8), with opposite sign; it follows that all terms cancel, obtaining Eq. (8). To define monopoles, let us introduce the function

$$m(x) = x - \lfloor x + 1/2 \rfloor\,. \tag{9}$$

It satisfies $-1/2 \le m(x) < 1/2$ and the relation $m(x) = x$ for any x in the interval $[-1/2, 1/2[$. Moreover $m(x) - x$ is always an integer. We can now define the number of monopoles/antimonopoles within the surface S as

$$N_{\rm mono}(S) = \sum_{P\in S} m\left(\frac{\Theta_{\boldsymbol{x},\mu}}{2\pi}\right). \tag{10}$$

Because of the relation (8), $N_{\rm mono}(S)$ is always an integer. Note that a nonvanishing number is only obtained if $|\Theta_{\boldsymbol{x},\mu}| > \pi$ on some plaquettes. Thus, a finite density of monopoles is only observed in the disordered high-temperature phase, up to the critical point. In the low-temperature phase, only isolated pairs of a monopole and an antimonopole are present. Their number decreases rapidly with increasing β, since $\theta_{\boldsymbol{x},\mu} = 0 \pmod{2\pi}$ on all plaquettes for $\beta \to \infty$.

To define a monopole-free version of the CP^{N-1} model, which we name $MFCP^{N-1}$, we restrict our configuration space, considering only configurations for which $N_{\rm mono}(C) = 0$ on any elementary lattice cube.

III. THE OBSERVABLES

In our numerical study we consider cubic lattices of linear size L with periodic boundary conditions. We simulate the system using the same overrelaxation algorithm

we employed in our previous work [21, 28]. It consists in a stochastic mixing of microcanonical and standard Metropolis updates of the lattice variables [29]. The only difference is the addition of a check: if the proposed move generates a monopole, the move is rejected.

We compute the energy density and the specific heat, defined as

$$E = \frac{1}{NV}\langle H\rangle, \qquad C = \frac{1}{N^2V}\left(\langle H^2\rangle - \langle H\rangle^2\right), \quad (11)$$

where $V = L^3$. We consider correlations of the gauge invariant operator $Q^{ab}_{\boldsymbol{x}}$ defined in Eq. (5). Its two-point correlation function is defined as

$$G(\boldsymbol{x}-\boldsymbol{y}) = \langle \mathrm{Tr}\, Q^\dagger_{\boldsymbol{x}} Q_{\boldsymbol{y}}\rangle, \quad (12)$$

where the translation invariance of the system has been taken into account. The susceptibility and the correlation length are defined as

$$\chi = \sum_{\boldsymbol{x}} G(\boldsymbol{x}) = \widetilde{G}(\boldsymbol{0}), \quad (13)$$

$$\xi^2 \equiv \frac{1}{4\sin^2(\pi/L)}\frac{\widetilde{G}(\boldsymbol{0}) - \widetilde{G}(\boldsymbol{p}_m)}{\widetilde{G}(\boldsymbol{p}_m)}, \quad (14)$$

where $\widetilde{G}(\boldsymbol{p}) = \sum_{\boldsymbol{x}} e^{i\boldsymbol{p}\cdot\boldsymbol{x}} G(\boldsymbol{x})$ is the Fourier transform of $G(\boldsymbol{x})$, and $\boldsymbol{p}_m = (2\pi/L, 0, 0)$. In our FSS analysis we use renormalization-group invariant quantities. We consider

$$R_\xi = \xi/L \quad (15)$$

and the Binder parameter

$$U = \frac{\langle \mu_2^2\rangle}{\langle \mu_2\rangle^2}, \qquad \mu_2 = \frac{1}{V^2}\sum_{\boldsymbol{x},\boldsymbol{y}} \mathrm{Tr}\, Q^\dagger_{\boldsymbol{x}} Q_{\boldsymbol{y}}. \quad (16)$$

We also consider the gauge-invariant vector correlation function [21, 28]

$$G_V(t,L) = \frac{1}{3V}\sum_{\boldsymbol{x},\mu} \mathrm{Re}\left\langle \bar{z}_{\boldsymbol{x}}\cdot z_{\boldsymbol{x}+t\hat{\mu}} \prod_{k=0}^{t-1} \lambda_{\boldsymbol{x}+k\hat{\mu},\hat{\mu}}\right\rangle . \quad (17)$$

IV. NUMERICAL RESULTS

A. Phase behavior for $N = 4, 10, 15$

We begin by discussing the behavior of the model for $N = 4, 10$, and 15. As we shall discuss, all results are consistent with a first-order transition. In Fig. 1 we show the behavior of the specific heat as a function of β. It shows clearly a maximum that becomes larger and larger which increasing L, signaling the presence of a phase transition. An estimate of the transition temperature can be obtained by analyzing the Binder parameter U as a function of β. Irrespective of the nature of the transition —it may be of first order or continuous— the curves corresponding to different sizes intersect at a

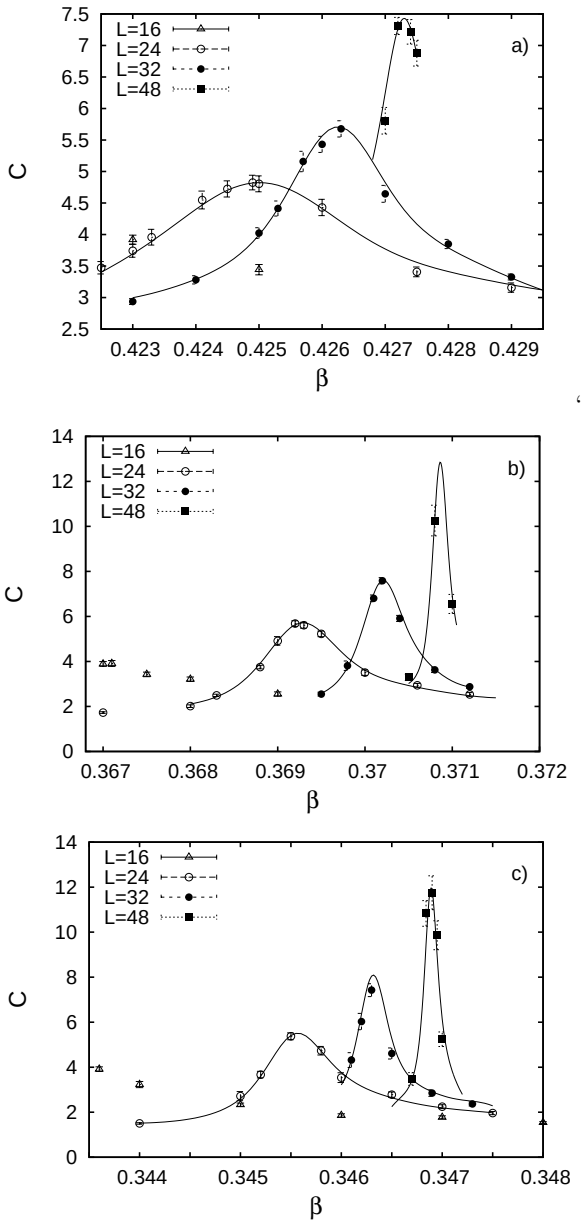


FIG. 1: Estimates of C versus β for the MFCP^{N-1} model for $N = 4$ (top, a), $N = 10$ (middle, b), $N = 15$ (bottom, c) and several lattice sizes L up to $L = 48$. The lines interpolating the data with $L = 24, 32$, and 48 are obtained using the multihistogram reweighting method [30].

temperature that converges to the transition temperature as $L \to \infty$. We obtain $\beta_c = 0.4285(5), 0.3712(3)$, and $0.3472(3)$ for $N = 4, 10, 15$, respectively. These results are significantly lower that the transition values for the model in which monopoles are allowed [20, 21]: $\beta_c = 0.5636(1), 0.4253(5), 0.381(1)$ for the same values of N. This decrease of β_c is expected, since the suppression of monopoles gives rise to an effective ordering interaction, that makes the high-temperature phase less stable.

From the data reported in Fig. 1, we can estimate the

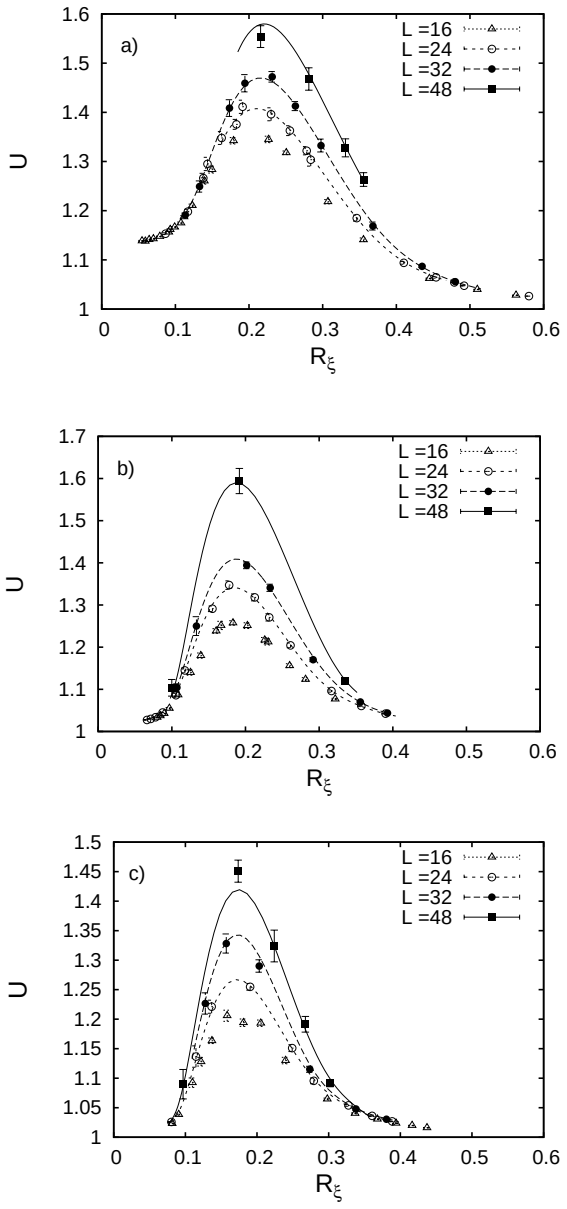


FIG. 2: Estimates of U versus R_ξ for the MFCP^{N-1} model for $N = 4$ (top, a), $N = 10$ (middle, b), $N = 15$ (bottom, c) and several lattice sizes L up to $L = 48$. The continuous lines interpolating the data with $L = 24, 32$, and 48 are obtained using the multihistogram reweighting method [30].

maximum $C_{\rm max}(L)$ of the specific heat. At a first-order transition, it behaves as

$$C_{\rm max}(L) = \frac{1}{4}\Delta_h^2 V \left[1 + O(V^{-1})\right], \qquad (18)$$

where $V = L^d$ is the d-dimensional volume ($d = 3$) and Δ_h is the latent heat. At a continuous transition, instead, we have

$$C_{\rm max}(L) = aL^{\alpha/\nu} + C_{\rm reg}, \qquad (19)$$

where the constant term $C_{\rm reg}$ is due to the analytic background. It is the dominant contribution if $\alpha < 0$. If we fit $C_{\rm max}(L)$ with a simple power behavior aL^δ, we obtain $\delta = 0.7(2)$, $1.3(2)$, $1.1(3)$ for $N = 4, 10, 15$. This behavior is quite different from that expected at a first-order transition ($\delta = d = 3$). If we assume that the transition is continuous, we should have $\delta = \alpha/\nu$, which would give $\nu = 0.54(3)$, $0.47(3)$, $0.49(4)$ (we use the hyperscaling relation $2 - \alpha = d\nu$) for $N = 4, 10, 15$, respectively.

The large difference between the estimates of δ and the first-order prediction $\delta = 3$ might be taken, a priori, as an indication that the transition is continuous. However, experience with similar models that undergo weak first-order transitions indicates that in many cases the analysis of the specific heat is not conclusive. The behavior (18) may set in at values of L that are much larger than those at which simulations can be actually performed. In the case of weak first-order transitions, a more useful quantity is the Binder parameter U. At a first-order transition, the maximum $U_{\rm max}(L)$ of U for each size L behaves as [31, 32]

$$U_{\rm max}(L) = c\, V \left[1 + O(V^{-1})\right] . \qquad (20)$$

On the other hand, U is bounded as $L \to \infty$ at a continuous phase transition. Indeed, at such transitions, in the FSS limit, any renormalization-group invariant quantity R scales as

$$R(\beta, L) = f_R(X) + O(L^{-\omega}), \quad X = (\beta - \beta_c)L^{1/\nu}, \qquad (21)$$

where $f_R(X)$ is a regular function, which is universal apart from a trivial rescaling of its argument, and ω is a correction to scaling exponent. Therefore, U has a qualitatively different scaling behavior for first-order or continuous transitions. In practice, a first-order transition can be simply identified by verifying that $U_{\rm max}(L)$ increases with L, without the need of explicitly observing the linear behavior in the volume.

In the case of weak first-order transitions, the nature of the transition can also be understood from the combined analysis of U and R_ξ [20]. At a continuous transition, in the FSS limit the Binder parameter U (more generally, any renormalization-group invariant quantity) can be expressed in terms of R_ξ as

$$U(\beta, L) = F_R(R_\xi) + O(L^{-\omega}), \qquad (22)$$

where $F_R(x)$ is universal. This scaling relation does not hold at first-order transitions, because of the divergence of U for $L \to \infty$. Therefore, the order of the transition can be understood from plots of U versus R_ξ. The absence of a data collapse is an early indication of the first-order nature of the transition, as already advocated in Ref. [20].

To understand the order of the transition, in Fig. 2 we report the Binder parameter as a function of R_ξ. The observed behavior is not consistent with a continuous transition. Data do not scale and moreover, the Binder parameter has a maximum that increases with the size

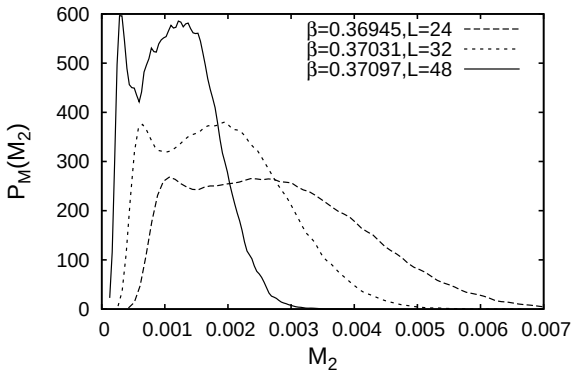


FIG. 3: Distribution $P_M(M_2)$ for the MFCP^9 model for different values of L. For each value of L we report the distribution for the value of β at which $P_M(M_2)$ has two peaks of approximately the same height. The distributions are obtained using the multihistogram reweighting method [30].

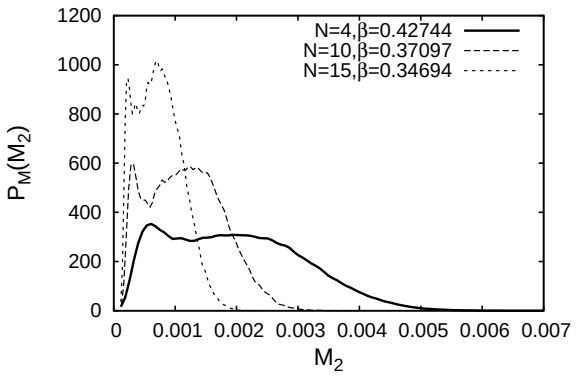


FIG. 4: Distribution $P_M(M_2)$ for the MFCP^{N-1} model for $L = 48$ and different values of N. For each value of N we report the distribution for the value of β at which $P_M(M_2)$ has two peaks of approximately the same height. The distributions are obtained using the multihistogram reweighting method [30].

L, a behavior that can only be observed at first-order transitions.

To further confirm the discontinuous nature of the transition we have studied the distributions of the order parameter and of the energy:

$$P_E(E) = \langle \delta[E - H/(NV)] \rangle, \qquad (23)$$
$$P_M(M_2) = \langle \delta(M_2 - \mu_2) \rangle,$$

where μ_2 is defined in Eq. (16). In Fig. 3 we show $P_M(M_2)$ for $N = 10$ and several values of L. For each size, we consider the value of β at which the distribution shows two peaks of approximately the same height $P_{\max}$. As expected for a first-order transition, if $P_{\min}$ is the minimum of the distribution between the two maxima, we observe that the ratio $P_{\max}/P_{\min}$ increases with L. This increase is not consistent with a continuous transition.

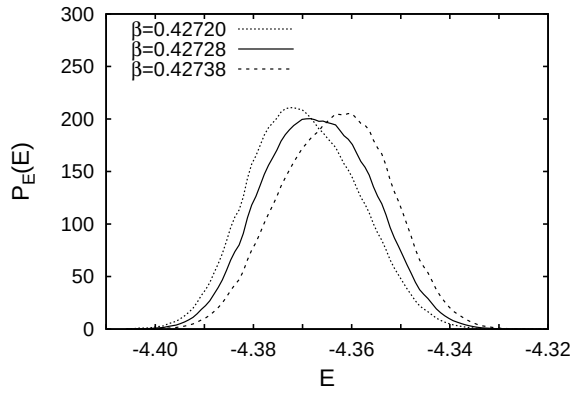


FIG. 5: Distribution $P_E(E)$ for the MFCP^3 model for $L = 48$ and different values of β. The distributions are obtained using the multihistogram reweighting method [30].

Indeed, at such transitions the distribution $P_M(M_2)$ may have two peaks — this is the case for the 3D Ising model [33]. However, in the Ising case the ratio $P_{\max}/P_{\min}$ is constant in the large-L limit. It is worth noting that the transition is very weak. The ratio $P_{\max}/P_{\min}$ is only slightly larger than one (the dip is barely significant if we take statistical errors into account) for $L = 24$, and is approximately equal to 1.2 and 1.4 for $L = 32$ and 48. This implies that there is still a significant overlap between the two phases, which explains the strong size dependence of the distribution. It is important to note that the distribution has two peaks only in a very tiny β interval. For $L = 48$, they are observed only when β belongs to the interval $[0.3709, 0.3710]$. Therefore, we made extensive use of the multihistogram method of Ref. [30], which allowed us to compute the distributions on a very fine grid of β values.

For both $N = 4$ and $N = 15$, the transition is weaker than for $N = 10$. We observe two peaks only for $L = 48$ in the first case and for $N = 32, 48$ in the second one. This is evident from the results reported in Fig. 4, where we show results for different values of N and $L = 48$. For $N = 4$ two peaks are barely visible, while for $N = 15$ we have $P_{\max}/P_{\min} \approx 1.15$. As a second remark, note also that the distributions become more narrow as N increases, indicating that the spontaneous magnetization decreases as N becomes large. We have also studied the distributions for the energy. For $N = 4$ a double-peak structure is not observed even for $L = 48$, although there is some evidence of two-phase behavior, see Fig. 5. A double-peak structure is instead observed for both $N = 10$ and $N = 15$.

B. Results for $N = 2$

Let us now discuss the results for $N = 2$. In this case we have not been able to draw any definite conclusion on the order of the transition. We have performed extensive

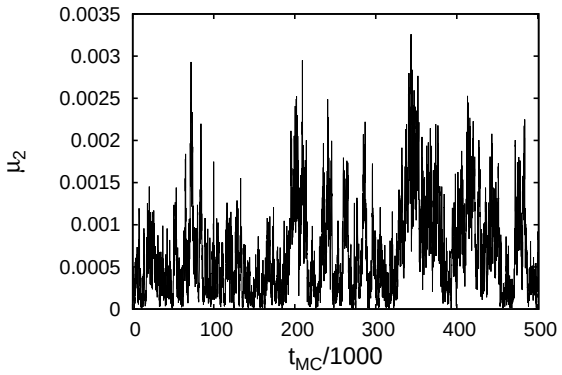


FIG. 6: Time evolution of μ_2 for $\beta = 0.4598$, $L = 80$, $N = 2$. Time is measured in lattice sweeps. We report the results for a time interval of $5 \cdot 10^5$ sweeps.

simulations on lattices of size up to $L = 80$. Each data point consists in $N_{\rm sw}$ lattice sweeps, with $N_{\rm sw}$ varying between 10^6 and $5 \cdot 10^6$. In spite of the large number of iterations, the statistics is not large, especially for $L \geq 48$, since autocorrelation times are huge. For $L = 64$ and 80, the integrated autocorrelation time associated with μ_2 [see Eq. (16)] is of order 3000 and 5000 iterations, respectively, in the transition region, so that the number of independent configurations varies between 500 and 1000 for these two values of L. The presence of strong autocorrelations can be easily understood by looking at the time dependence of μ_2 reported in Fig. 6. Typical configurations are not magnetized—μ_2 is very small—but, at intervals of the order of 10^3-10^4 iterations, a fluctuation occurs towards configurations of larger magnetization. In order to improve the quality of the results, we have extensively used the multihistogram method of Ref. [30], combining all runs corresponding to the same size L.

In Fig. 7 we report the specific heat C and the Binder parameter U as a function of β. The parameter U shows an intersection for $\beta \approx 0.4605$, indicating the presence of a phase transition. In the same β region the specific heat has a peak that increases with the size L. For each value of L we have determined $C_{\rm max}(L)$. A fit of the results for $L \geq 48$ to aL^δ gives $\delta = 0.35(8)$. We have also performed a fit including an analytic correction, fitting $\ln C_{\rm max}(L)$ to $\delta \ln L + a + bL^{-\delta}$. Using the results for $L \geq 32$ we obtain $\delta = 0.7(2)$. The exponent δ is quite different from what one would expect for a first-order transition, $\delta = 3$. If the transition is continuous, δ should be identified with α/ν. Using the hyperscaling relation $2 - \alpha = 3\nu$, we would then predict $\nu = 0.60(2)$ and 0.54(3), using the two results for δ. Note that the results for the specific heat exclude a critical transition in the O(3) universality class, since $\alpha < 0$ for the latter model [34].

To understand the nature of the transition, in Fig. 8 we report U versus R_ξ. In this case, the plot does not allow us to draw any definite conclusion. On one side, the data do not scale: At fixed R_ξ, the estimates of U

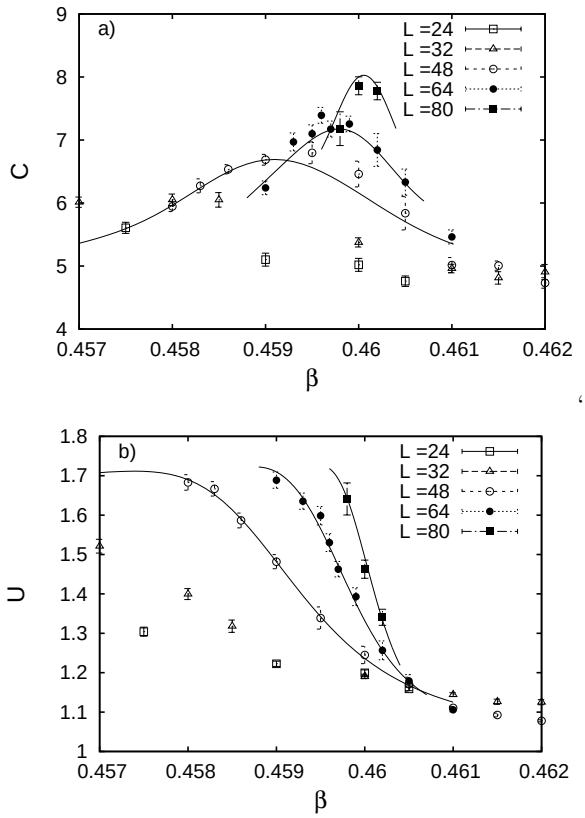


FIG. 7: Plot of the specific heat C (top, a) and of the Binder parameter U (bottom, b) as a function of β in the transition region. Results for several values of L up to $L = 80$ for $N = 2$. The curves (continuous lines) interpolating the data with $L = 48$, 64, and 80 are obtained using the multihistogram reweighting method [30].

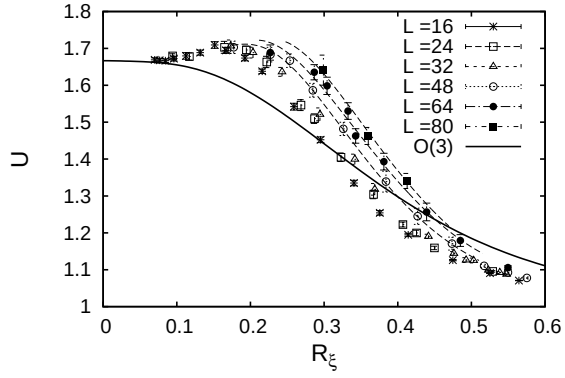


FIG. 8: Plot of the Binder parameter U versus R_ξ, for several values of L up to $L = 80$ for $N = 2$. The curves (dashed lines) interpolating the data with $L = 48$, 64, and 80 (L increases moving rightward) are obtained using the multihistogram reweighting method [30]. The continuous thicker line is the universal curve for the O(3) universality class [35].

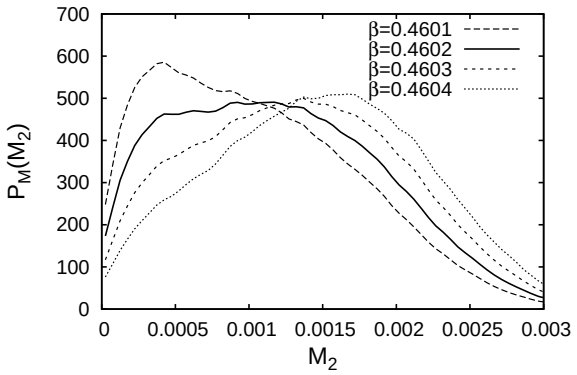


FIG. 9: Distribution $P_M(M_2)$ for the MFCP[1] model for $L = 80$ and three different values of β. The distributions are obtained using the multihistogram reweighting method [30].

are systematically increasing with L for $0.2 \le R_\xi \lesssim 0.5$. This would favor a first-order transition. On the other hand, the estimates of U do not show a maximum that increases with L. This behavior is usually taken as an indication for a continuous transition, although the recent results of Ref. [36] show that it is possible to have a discontinuous transition even when the Binder parameter does not show a peak for lattice sizes that are usually considered quite large (they perform simulations up to $L = 256$). Whatever the interpretation be, O(3) behavior is clearly excluded, as already noted from the analysis of the specific heat.

We have also computed the distributions of μ_2. We do not observe any double-peak structure. However, as β varies, the distributions change as expected for a first-order transition, see Fig. 9. Indeed, for $\beta = 0.4901$, $P_M(M_2)$ has a peak for $M_2 = 0.0004$, for $\beta = 0.4902$ the curve flattens, and then is starts showing a new distinct maximum at $M_2 \approx 0.002$ as β increases. This behavior is consistent with what is observed in Fig. 6. The large fluctuations can be interpreted as the typical see-saw behavior observed in the presence of two distinct coexisting phases. The system moves between the unmagnetized phase ($\mu_2 \sim 10^{-4}$) and a magnetized phase with $\mu_2 \approx 0.002$.

To conclude the analysis of the available data, we may assume that the transition is continuous and determine the critical exponents. First, we determine ν and the transition value β_c fitting the data to Eq. (21). The function $f_R(x)$ is approximated by a polynomial. The results of the fits are reported in Table I as a function of $L_{\rm min}$, the minimum size of the data included in the fit. We observe a significant drop of the estimate of ν as $L_{\rm min}$ increases from 24 to 32. This is due to the large scaling corrections we have already observed when considering U versus R_ξ, Moreover, the estimates of β_c obtained by using R_ξ and U are not consistent within errors. If we

TABLE I: Results of the fits to Eq. (21) for different values of $L_{\rm min}$, the minimum size of the data included in the fit. For the function $f(x)$ we take a twelfth-order polynomial for $L_{\rm min} = 24$ and 32, and a sixth-order polynomial for $L_{\rm min} = 48$. Here χ^2 is the sum of the fit square residuals and DOF is the number of degrees of freedom.

	$L_{\rm min}$	χ^2/DOF	ν	β_c
U_4	24	39/33	0.547(5)	0.46057(3)
	32	22/22	0.516(17)	0.46054(4)
	48	8/14	0.56(6)	0.46066(10)
R_ξ	24	160/33	0.594(4)	0.46035(1)
	32	58/22	0.527(9)	0.46030(2)
	48	6/14	0.53(3)	0.46040(5)

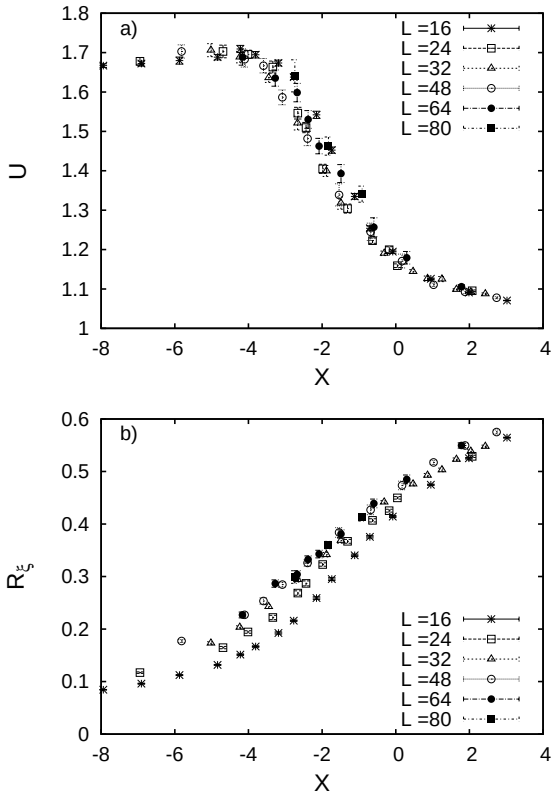


FIG. 10: Plot of U (top, a) and of R_ξ (bottom, b) as a function of $X = (\beta - \beta_c)L^{1/\nu}$, using $\beta_c = 0.4605$ and $\nu = 0.52$, the estimates (24).

average the results of the two analyses, we would estimate

$$\nu = 0.52(2), \qquad \beta_c = 0.4605(3). \tag{24}$$

In Fig. 10 we report the corresponding scaling plots. As expected, the quality of the scaling is poor: large deviations are present. In any case, note that the estimate of ν is consistent with that obtained from the specific heat, $\nu = 0.54(3)$, obtained including the analytic corrections.

Finally, we determine the exponent η associated with the susceptibility χ defined in Eq. (13). This quantity

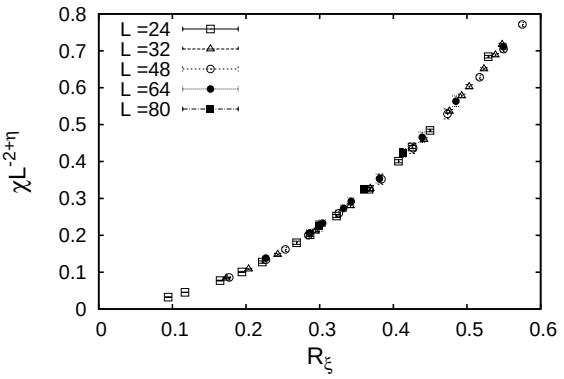


FIG. 11: Plot of $\chi/L^{2-\eta}$ as a function of R_ξ, using $\eta = 0.335$.

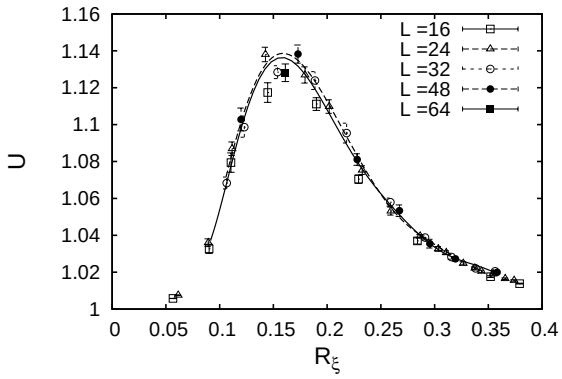


FIG. 12: Plot of the Binder parameter U versus R_ξ, for several values of L up to $L = 64$ for $N = 25$. The curves interpolating the data with $L = 32$ (dashed line) and 48 (continuous line) are obtained using the multihistogram reweighting method [30].

scales as

$$\chi(\beta, L) \sim L^{2-\eta} \left[f_\chi(X) + O(L^{-\omega}) \right], \qquad (25)$$

or, equivalently, as

$$\chi(\beta, L) \sim L^{2-\eta} \left[F_\chi(R_\xi) + O(L^{-\omega}) \right]. \qquad (26)$$

We therefore fit the data to $\ln \chi = (2-\eta) \log L + \hat{f}_\chi(R_\xi)$, where we approximate the function $\hat{f}_\chi(x)$ with a polynomial in x. To estimate the role of the scaling corrections we include in the fit only the data corresponding to sizes $L \geq L_{\rm min}$. We obtain $\eta = 0.352(7)$ and $0.335(10)$ for $L_{\rm min} = 24$ and 32, respectively. In this case, scaling corrections appear to be small (χ^2/DOF is approximately 0.99 for $L_{\rm min} = 24$ and 0.56 for $L_{\rm min} = 32$; DOF is the number of degrees of freedom of the fit), as is also evident from the scaling plot, Fig. 11. Conservatively, we will take $\eta = 0.335(10)$ as our final estimate.

In conclusion the results for $N = 2$ may be still interpreted in terms of two different scenarios. A first possibility is that the transition is of first order. This would explain the poor scaling we observe when we plot U versus R_ξ, the inconsistencies in the results of ν and β_c obtained in the analysis of U and R_ξ, and the shape of the distribution of the order parameter, see Fig. 9. However, the absence of a divergence in the behavior of the Binder parameter does not allow us to exclude that the transition is continuous and that the observed inconsistencies are simply due to scaling corrections that are particularly large in this model. A continuous transition is also supported by the behavior of the susceptibility that shows a good scaling, which allows us to obtain an apparently accurate estimate of the exponent η. If the transition is continuous, it does not belong to the Heisenberg universality class: O(3) behavior is clearly excluded by the data.

C. Results for $N = 25$

We finally present our results for $N = 25$. We have performed simulations on lattices of size $16 \leq L \leq 64$.

TABLE II: Results of the fits to Eq. (21), as a function of $L_{\rm min}$. For the function $f_R(x)$ we take a twelfth-order polynomial. Results for the MFCP^{24} model.

	$L_{\rm min}$	χ^2/DOF	ν	β_c
R_ξ	16	89/31	0.579(2)	0.319943(3)
	24	39/23	0.597(4)	0.319963(5)
U_4	16	112/31	0.567(5)	0.319938(10)
	24	48/23	0.593(9)	0.319969(13)

Autocorrelations are very large (of the order of 10^3 for $L = 64$), so that simulations of larger lattices are unfeasible. Note that most of the data correspond to $L \leq 48$. For $L = 64$ we have a single data point. As we shall discuss, all results are consistent with a continuous transition.

We first analyze the behavior of the Binder parameter and of the specific heat as a function of β. The specific heat shows a very clear maximum that increases with L and the Binder parameter curves at fixed L have a crossing point for $\beta \approx 0.320$, which allows us to identify the transition region. To determine the order of the transition, we consider the plot of U versus R_ξ, see Fig. 12. It is quite evident that all results approximately fall onto a single curve with small scaling corrections. This is confirmed by the curves obtained by using the multihistogram reweighting method of Ref. [30]: the curves corresponding to $L = 32$ and 48 cannot be distinguished on the scale of figure except at the peak. Note that the curves apparently indicate that $U_{\rm max}(L)$ decreases as L is increased, which is the opposite behavior of that expected at first-order transitions. The downward trend at the peak is also confirmed by the result obtained for $L = 64$: the estimate of U is lower than the $L = 48$ curve, see Fig. 12. We can thus exclude that the transition is of first order.

Next, we determine the critical exponents. We fit the

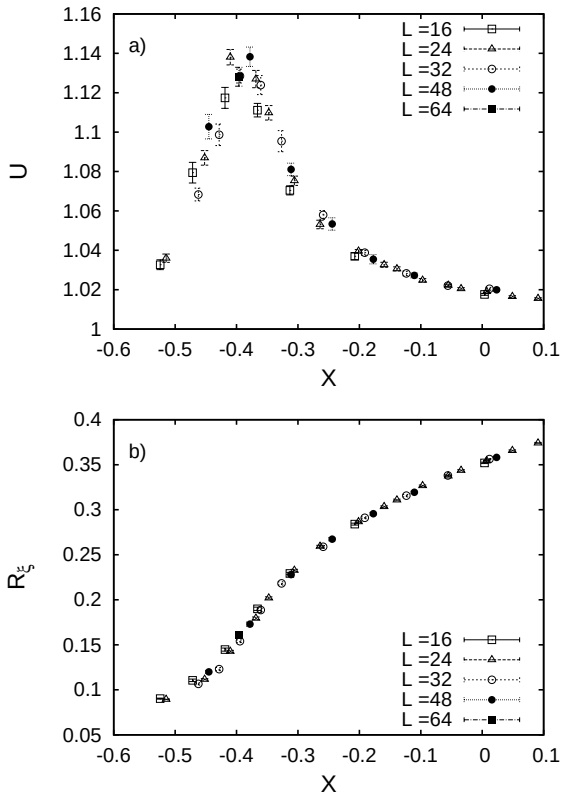


FIG. 13: Plot of U (top, a) and of R_ξ (bottom, b) as a function of $X = (\beta - \beta_c)L^{1/\nu}$, using $\beta_c = 0.319965$ and $\nu = 0.595$. Results for the MFCP^{24} model.

results for U and R_ξ to Eq. (21). We approximate $f_R(x)$ with a 12th-order polynomial. The results of the fits are reported in Table II as a function of $L_{\rm min}$, the minimum size of the data included in the fit. There is some dependence on $L_{\rm min}$, due to scaling corrections. For $L_{\rm min} = 24$, the estimates obtained from R_ξ and U are consistent, so that we can finally estimate

$$\beta_c = 0.319965(20), \qquad \nu = 0.595(15). \tag{27}$$

Errors should be considered as conservative. They are obtained by requiring consistency between the results obtained for the two values of $L_{\rm min}$. The data are reported in Fig. 13 as a function of $X = (\beta - \beta_c)L^{1/\nu}$. Scaling is quite good, especially for the correlation-length ratio. As a consistency check, we have determined ν using the specific heat. We find that the the maximum of the specific heat $C_{\rm max}(L)$ scales as L^δ with $\delta = 0.46(15)$. It implies $\nu = 0.58(3)$, which is consistent with Eq. (27).

We also study the critical behavior of the susceptibility χ, performing fits to the ansatz

$$\ln \chi = (2 - \eta) \ln L + \hat{f}_\chi(R_\xi). \tag{28}$$

We obtain $\eta = 0.929(3), 0.868(5), 0.871(11)$ for $L_{\rm min} = 16, 24, 32$. Note that the results for the two largest values of L are consistent, allowing us to estimate

$$\eta = 0.87(1). \tag{29}$$

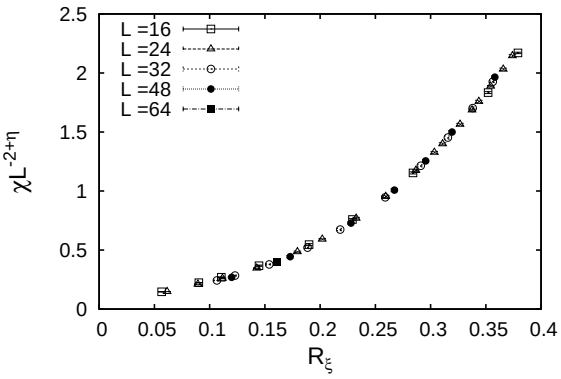


FIG. 14: Plot of $\chi/L^{2-\eta}$ as a function of R_ξ, using $\eta = 0.87$. Results for the MFCP^{24} model.

In Fig. 14 we report $\chi/L^{2-\eta}$ versus R_ξ. The quality of the scaling is excellent.

Finally, we analyze the behavior of the correlation function $G_V(x)$. We find that $G_V(x)$ behaves as $A \exp(-x/\xi_z)$, where the correlation length ξ_z varies between 2.7 and 3.5 in the critical region for any L in the interval $24 \le L \le 64$. Similar results are obtained also for $N = 4, 10, 15$. In all cases ξ_z is small: we find $\xi_z = 2.1(1), 2.6(1), 2.8(1)$, for $N = 4, 10, 15$, respectively, where the error takes into account the L and β dependence in the transition region. For finite N, the correlation ξ_z is expected to be finite [37–39]. It should, however, diverge in the limit $N \to \infty$, as in this limit the gauge degrees of freedom are frozen and $\lambda_{\boldsymbol{x},\mu}$ can be taken equal to 1. The smallness of ξ_z for $N = 25$ indicates that we are still quite far from the large-N limit.

V. CONCLUSIONS

This paper reports a study of the phase diagram, and the nature of the phase transitions, of 3D lattice MFCP^{N-1} models characterized by a global U(N) symmetry and a U(1) gauge symmetry, and the absence of monopoles. We consider the usual lattice nearest-neighbor formulation of the CP^{N-1} model with an explicit gauge field—the corresponding Hamiltonian is given in Eq. (1)—restricting the configuration space to gauge-field configurations in which no monopoles are present. To define monopoles, we use the definition proposed by De Grand and Toussaint [26]. To determine the phase diagram of the 3D MFCP^{N-1} model we perform Monte Carlo simulations for $N = 2$, 4, 10, 15, and 25. The analysis of the finite-size data allows us to identify a finite-temperature transition in all cases, related to the condensation of a local gauge-invariant bilinear order parameter $Q_{\boldsymbol{x}}$, cf Eq. (5).

For $N = 2$ we considered lattices of size up to $L = 80$. In spite of the relatively large systems considered, we are unable to draw a definite conclusion on the nature of the

transition. We can only safely exclude that the transition belongs to the O(3) universality class, as it occurs in the CP^1 model in which monopoles are allowed. Some results show features that are typical of first-order transitions: the results for the Binder parameter U do not approach a universal curve when plotted versus $R_\xi = \xi/L$, and the distributions of the order parameter and of the energy are quite broad, although without the typical two-peak shape that signals the presence of two coexisting phases. On the other hand, we do not observe an increase of the maximum $U_{\max}(L)$ of the Binder parameter, which is a signature of a first-order transition, so that a continuous transition is not excluded.

If we assume that the $MFCP^1$ has a continuous transition, we can estimate the critical exponents. For the correlation-length exponent ν, the quality of the FSS fits is poor. The exponent significantly decreases as the smallest-volume data are excluded from the fit, a phenomenon that is often considered as the signature of a weak first-order transition: in these cases ν decreases towards $1/d = 1/3$ as larger size data are included. If we only consider the largest sizes, we would estimate $\nu = 0.52(2)$, but it is clear from the quality of the fits that this estimate should be only considered as an effective estimate in the range of values of L considered. It remains an open problem to establish if such a drift stops and the estimate stabilizes, as appropriate for a continuous transition, or moves towards the first-order value 1/3. The exponent ν can also be determined from the specific heat, using the hyperscaling relation $2 - \alpha = 3\nu$. We obtain $\nu = 0.54(3)$, which is consistent with the previous estimate. We have also analyzed the behavior of the susceptibility χ of the order parameter $Q_{\boldsymbol{x}}$. In this case, we observe good scaling and little size dependence of the results. We estimate $\eta = 0.335(10)$. The good scaling of χ is presently the only real evidence in favor of a continuous transition.

It is interesting to compare these results with those obtained in other models. An O(3) σ model with hedgehog suppression was considered in Ref. [24]. The estimates of ν and η are different from ours, as they obtain $\nu = 1.0(2)$ and $\eta \approx 0.6$. The $MFCP^1$ and the model of Ref. [24] have the same global symmetry and the same order parameter, but consider different types of topological defects; therefore, they may develop a different behavior. A loop model, expected [40, 41] to have the share the same universal large-distance behavior with the $MFCP^1$, was considered in Ref. [7]. The numerical results obtained on very large systems (up to $L = 512$) show some similarities, but also some notable differences, with ours. For instance, they also find significant violations of FSS and a significant dependence of the estimates of ν from the system sizes considered. The loop-model estimates of ν vary from 0.6 at small sizes to $\nu \approx 0.46$ for the largest ones. We can also compare our estimate of η with that obtained in Ref. [7] for the Néel order parameter, which corresponds to our operator $Q_{\boldsymbol{x}}$. The FSS analysis of the order parameter or of the corresponding susceptibility shows significant FSS violations. On the other hand, the analysis of the short-distance behavior of the two-point correlation function gives a quite clear power-law behavior up to distances $r \sim 100$ with quite good scaling collapse. This allows Ref. [7] to estimate $\eta = 0.259(6)$, which, however, significantly differs from our estimate $\eta = 0.335(10)$. This difference may be explained either by a different universality class or by the fact that at least one of the two models does not undergo a continuous transition. Of course, it is also possible, as suggested in the literature on quantum antiferromagnets, that the transition is continuous with anomalously large and slowly decaying—even logarithmic [12], associated with a dangerously irrelevant variable—scaling corrections.

The results for $N = 4, 10$, and 15 are instead quite conclusive on the order of the transition. In all cases, we have clear evidence that the transition is of first order. The maximum $U_{\max}(L)$ of the Binder parameter increases with L and, for sufficiently large L, we observe two maxima in the distributions of the order parameter and of the energy (for the energy only for $N = 10, 15$). The transition is significantly weaker than in the usual CP^{N-1} model in which monopoles are allowed. In particular, while in the latter model the transition becomes stronger as N increases, for the $MFCP^{N-1}$ the opposite occurs for $N \geq 10$: the transition for $N = 10$ is stronger than for $N = 15$. As expected for first-order transitions, the maximum $C_{\max}(L)$ of the specific heat diverges. In our range of values of L, however, the increase is slower than the expected one, $C_{\max}(L) \sim L^d = L^3$. Apparently, it increases as L^δ, with $\delta \sim 1$, which would imply, using the usual relations valid for continuous transitions, an effective exponent ν of the order of 0.5. This shows that effective estimates of ν around 1/2 are not uncommon in the presence of weak first-order transitions, casting additional doubts on the interpretation of the results for $N = 2$ as a continuous transition.

Our conclusions for the nature of the transition for $4 \leq N \leq 15$ differ from those of Refs. [5, 6], that observed instead continuous transitions in the same range of values of N. Note, however, that this is not necessarily an inconsistency. A priori, it is always possible that a $MFCP^{N-1}$ fixed point exists for these values of N, but that our model is outside its attraction domain. We mention that the existence of a range of value of N, where the model undergoes a weakly first-order transition is consistent with the renormalization-group analysis of Ref. [46].

Finally, we have studied the $MFCP^{N-1}$ model with $N = 25$. In this case, data are consistent with a conventional continuous transition. Data (with L up to 64) show a good FSS, with exponents

$$\nu = 0.595(15), \qquad \eta = 0.87(1). \tag{30}$$

It is interesting to compare our results with the predictions of the field-theory approaches that are used to describe the large-distance behavior of the model: the gauge-invariant Landau-Ginzburg-Wilson (LGW) ap-

TABLE III: Estimates of the transition point for the CP^{N-1} model with monopoles (β_c^{std}), taken from Refs. [20, 21], and for the $MFCP^{N-1}$ model without monopoles (β_c).

N	β_c	$\beta_c^{\rm std}$
2	0.4605(3)	0.7102(1)
4	0.4285(5)	0.5636(1)
10	0.3712(3)	0.4253(5)
15	0.3472(3)	0.381(1)
20		0.353(2)
25	0.319965(20)	

proach, see Ref. [20, 28], which has also been successfully applied to systems with nonabelian gauge symmetries [42, 43], and the Abelian-Higgs field theory [27, 44–46]. The first approach predicts a first-order transition for $N \geq 3$. For $N = 2$, continuous transitions necessarily belong to the O(3) universality class. Our results are clearly not consistent with the LGW predictions, as we find a continuous transition for $N = 25$ (the results for $N = 2$ might still be consistent with the LGW approach if the phase transition of the $MFCP^1$ model is of first order). This shows that the LGW approach is not appropriate to describe the monopole-free model. However, this is not surprising. If monopoles are relevant in defining the long-distance behavior of the model, the effective theory should include somehow the information on the topology of the gauge fields. This is clearly not possible in the LGW approach, as the gauge degrees of freedom are integrated out.

The Abelian-Higgs field theory [44] predicts continuous transitions for $N > N_{c,FT}$ and first-order ones for $N < N_{c,FT}$. Close to 4 dimensions, we have [44] $N_{c,FT} \approx 183$. A three-dimensional estimate is quite problematic to obtain, because of the non-Borel summability of the perturbative series in powers of $\epsilon = 4-d$. Ref. [46] quotes $N_{c,FT} = 12.2(3.9)$. It is tempting to conjecture that the continuous transition we have observed for $N = 25$ is associated with the stable large-N fixed point occurring in the Abelian-Higgs field theory. This would also be supported by the fact that our estimate of the value N_c separating first-order from continuous transitions, which should belong to the interval $15 < N_c < 25$, is essentially consistent with the field-theory estimate of Ref. [46].

Finally, let us consider the behavior for $N \to \infty$. In Ref. [21], we showed that the model with Hamiltonian (1) has a first-order transition for any $N \geq 3$, including $N = \infty$, contradicting the analytic computations of Ref. [18]. It was conjectured that the failure is due to the presence of monopoles in the disordered phase that do not allow the ordering of the gauge fields [25], even for $N = \infty$. If this interpretation is correct, the $MFCP^{N-1}$ model should instead give results consistent with the analytic computations of Ref. [18] in the large-N limit. The fact that the transition becomes continuous as N increases supports this conjecture. A more quantitative check can be performed using the large-N estimates [44, 47, 48]

$$\eta = 1 - \frac{32}{\pi^2 N}, \qquad \nu = 1 - \frac{48}{\pi^2 N}. \tag{31}$$

For $N = 25$ they give $\eta = 0.87$ and $\nu = 0.81$. The estimate of η is in perfect agreement with our result, while the estimate of ν differs considerably. This is, however, not totally surprising, since the critical value N_c where the order of the transition changes (consequently $1/N_c$ is expected to be the radius of the region in which the large-N expansion is predictive) may be close to 25. If this occurs, it is clear that a quantitative agreement requires considering several terms of the expansion. As a final remark, we note that the difference $\beta_c(N)^{\rm std} - \beta_c(N)$ ($\beta_c(N)^{\rm std}$ and $\beta_c(N)$ are the transition points for the model with and without monopoles, respectively, reported in Table III) scales quite precisely as $1/N$. This leads us to conjecture that, for $N = \infty$, monopoles do not change the transition temperature, but only the nature of the disordered high-temperature phase.

[1] N. Read and S. Sachdev, Spin-Peierls, valence-bond solid, and Néel ground states of low-dimensional quantum antiferromagnets, Phys. Rev. B **42**, 4568 (1990).

[2] S. Takashima, I. Ichinose, and T. Matsui, CP^1+U(1) lattice gauge theory in three dimensions: Phase structure, spins, gauge bosons, and instantons, Phys. Rev. B **72**, 075112 2005).

[3] S. Takashima, I. Ichinose, and T. Matsui, Deconfinement of spinons on critical points: Multiflavor CP^1+U(1) lattice gauge theory in three dimension, Phys. Rev. B **73**, 075119 (2006).

[4] R. K. Kaul, Quantum phase transitions in bilayer SU(N) antiferromagnets, Phys. Rev. B **85**, 180411(R) (2012).

[5] R. K. Kaul and A. W. Sandvik, Lattice Model for the SU(N) Néel to Valence-Bond Solid Quantum Phase Transition at Large N, Phys. Rev. Lett. **108**, 137201 (2012).

[6] M. S. Block, R. G. Melko, and R. K. Kaul, Fate of CP^{N-1} fixed point with q monopoles, Phys. Rev. Lett. **111**, 137202 (2013).

[7] A. Nahum, J. T. Chalker, P. Serna, M. Ortuño, and A. M. Somoza, Deconfined Quantum Criticality, Scaling Violations, and Classical Loop Models, Phys. Rev. X **5**, 041048 (2017).

[8] C. Wang, A. Nahum, M. A. Metliski, C. Xu, and T. Senthil, Deconfined Quantum Critical Points: Symmetries and Dualities, Phys. Rev. X **7**, 031051 (2017).

[9] A. W. Sandvik, Evidence for Deconfined Quantum Criticality in a Two-Dimensional Heisenberg Model with Four-Spin Interactions, Phys. Rev. Lett. **98**, 227202 (2007).

[10] R. G. Melko and R. K. Kaul, Scaling in the Fan of an Un-

conventional Quantum Critical Point, Phys. Rev. Lett. **100**, 017203 (2008).

[11] F. J. Jiang, M. Nyfeler, S. Chandrasekharan, and U. J. Wiese, From an Antiferromagnet to a Valence Bond Solid: Evidence for a First-Order Phase Transition, J. Stat. Mech. (2008) P02009.

[12] A. W. Sandvik, Continuous Quantum Phase Transition between an Antiferromagnet and a Valence-Bond Solid in Two Dimensions: Evidence for Logarithmic Corrections to Scaling, Phys. Rev. Lett. **104**, 177201 (2010); H. Shao, W. Guo, and A. W. Sandvik, Quantum criticality with two length scales, Science **352**, 213 (2016).

[13] K. Harada, T. Suzuki, T. Okubo, H. Matsuo, J. Lou, H. Watanabe, S. Todo, and N. Kawashima, Possibility of Deconfined Criticality in SU(N) Heisenberg Models at Small N, Phys. Rev. B **88**, 220408 (2013).

[14] K. C. Y. Huang, Y. Deng, A. B. Kuklov, N. V. Prokofiev, and B.V. Svistunov, Deconfined Criticality Flow in the Heisenberg Model with Ring-Exchange Interactions, Phys. Rev. Lett. **110**, 185701 (2013).

[15] S. Pujari, K. Damle, and F. Alet, Nèel-State to Valence-Bond-Solid Transition on the Honeycomb Lattice: Evidence for Deconfined Criticality, Phys. Rev. Lett. **111**, 087203 (2013).

[16] T. Senthil, L. Balents, S. Sachdev, A. Vishwanath, and M. P. A. Fisher, Quantum Criticality beyond the Landau-Ginzburg-Wilson Paradigm, Phys. Rev. B **70**, 144407 (2004).

[17] E. Rabinovici and S. Samuel, The CP^{N-1} model: A strong coupling lattice approach, Phys. Lett. **101B**, 323 (1981).

[18] P. Di Vecchia, A. Holtkamp, R. Musto, F. Nicodemi, and R. Pettorino, Lattice CP^{N-1} models and their large-N behaviour, Nucl. Phys. B **190**, 719 (1981).

[19] B. Berg and M. Lüscher, Definition and statistical distributions of a topological number in the lattice O(3) σ-model, Nucl. Phys. B **190**, 412 (1981).

[20] A. Pelissetto and E. Vicari, Three-dimensional ferromagnetic CP^{N-1} models, Phys. Rev. E **100**, 022122 (2019).

[21] A. Pelissetto and E. Vicari, Large-N behavior of three-dimensional lattice CP^{N-1} models, J. Stat. Mech.: Th. Expt. 033209 (2020).

[22] M. Lau and C. Dasgupta, Numerical investigation of the role of topological defects in the three-dimensional Heisenberg transition, Phys. Rev. B **39**, 7212 (1989).

[23] M. Kamal and G. Murthy, Phys. Rev. Lett. **71**, 1911 (1993).

[24] O. I. Motrunich and A. Vishwanath, Emergent photons and transitions in the O(3) σ-model with hedgehog suppression, Phys. Rev. B **10**, 075104 (2004).

[25] G. Murthy and S. Sachdev, Actions of hedgehogs instantons in the disordered phase of 2+1 dimensional CP^{N-1} model, Nucl. Phys. B **344**, 557 (1990).

[26] T. A. De Grand and D. Toussaint, Topological excitations and Monte Carlo simulation of Abelian gauge theory, Phys. Rev. D **22**, 2478 (1980).

[27] M. Moshe and J. Zinn-Justin, Quantum field theory in the large N limit: A review, Phys. Rep. **385**, 69 (2003).

[28] A. Pelissetto and E. Vicari, Multicomponent compact Abelian-Higgs lattice models, Phys. Rev. E **100**, 042134 (2019).

[29] To update each lattice variable, we randomly choose either a standard Metropolis update, which ensures ergodicity, or a microcanonical move, which is more efficient than the Metropolis one but does not change the energy. Typically, on average we perform four/three microcanonical updates for every Metropolis proposal. In the Metropolis update, changes are tuned so that the acceptance is approximately 1/3.

[30] A. M. Ferrenberg and R. H. Swendsen, Optimized Monte Carlo data analysis, Phys. Rev. Lett. **63**, 1195 (1989).

[31] M. S. S. Challa, D. P. Landau, and K. Binder, Finite-size effects at temperature-driven first-order transitions, Phys. Rev. B **34**, 1841 (1986).

[32] K. Vollmayr, J. D. Reger, M. Scheucher, and K. Binder, Finite size effects at thermally-driven first order phase transitions: A phenomenological theory of the order parameter distribution, Z. Phys. B **91**, 113 (1993).

[33] M. M. Tsypin and H. W. J. Blöte, Probability distribution of the order parameter for the three-dimensional Ising-model universality class: A high-precision Monte Carlo study, Phys. Rev. E **62** (2000) 73.

[34] A. Pelissetto and E. Vicari, Critical Phenomena and Renormalization Group Theory, Phys. Rep. **368**, 549 (2002).

[35] We have performed simulations in the usual O(3) vector model with periodic boundary conditions to determine the FSS curve of the Binder parameter $U = F(R_\xi)$. An interpolation is $F(x) = 1.666666 + x(3.0263535 + 23.139470x)(1 - e^{-15x}) - 47.838890x^2 + 58.489668x^3 - 67.020681x^4 + 38.408855x^5 - 8.8557348x^6$. The error is smaller than 0.5%.

[36] P. Serna and A. Nahum, Emergence and spontaneous breaking of approximate O(4) symmetry at a weakly first-order deconfined phase transition, Phys. Rev. B **99**, 195110 (2019).

[37] V. S. Dotsenko and S. N. Vergeles, Renormalizability of phase factors in non-abelian gauge theory, Nucl. Phys. B **169**, 527 (1980).

[38] S. Aoyama, The renormalization of the string operator in QCD, Nucl. Phys. B **194**, 513 (1982).

[39] M. Campostrini and P. Rossi, CP^{N-1} models in the $1/N$ expansion, Phys. Rev. D **45**, 618 (1992).

[40] A. Nahum, J. T. Chalker, P. Serna, M. Ortuño, and A. M. Somoza, 3D Loop Models and the CP^{N-1} Sigma Model, Phys. Rev. Lett. **107**, 110601 (2011).

[41] A. Nahum, J. T. Chalker, P. Serna, M. Ortuño, and A. M. Somoza, Phase transitions in three-dimensional loop models and the CP^{N-1} σ model, Phys. Rev. B **88**, 134411 (2013).

[42] R. D. Pisarski and F. Wilczek, Remarks on the chiral phase transition in chromodynamics, Phys. Rev. D **29**, 338 (1984).

[43] C. Bonati, A. Pelissetto, and E. Vicari, Phase Diagram, Symmetry Breaking, and Critical Behavior of Three-Dimensional Lattice Multiflavor Scalar Chromodynamics, Phys. Rev. Lett. **123**, 232002 (2019); Three-dimensional lattice multiflavor scalar chromodynamics: Interplay between global and gauge symmetries, Phys. Rev. D **101**. 034505 (2020).

[44] B. I. Halperin, T. C. Lubensky, and S. K. Ma, First-Order Phase Transitions in Superconductors and Smectic-A Liquid Crystals, Phys. Rev. Lett. **32**, 292 (1974).

[45] R. Folk and Y. Holovatch, On the critical fluctuations in superconductors, J. Phys. A **29**, 3409 (1996).

[46] B. Ihrig, N. Zerf, P. Marquard, I. F. Herbut, and M. M. Scherer, Abelian Higgs model at four loops, fixed-point collision and deconfined criticality, Phys. Rev. B **100**,

134507 (2019).

[47] V. Yu. Irkhin, A. A. Katanin, and M. I. Katsnelson, $1/N$ expansion for critical exponents of magnetic phase transitions in the CP^{N-1} model for $2 < d < 4$, Phys. Rev. B **54**, 11953 (1996).

[48] R. K. Kaul and S. Sachdev, Quantum criticality of U(1) gauge theories with fermionic and bosonic matter in two spatial dimensions, Phys. Rev. B **77**, 155105 (2008).